Behavioral/Cognitive

Homeostatic Coupling of Cortical and Brainstem Delta Rhythms in Sleeping Infant Rats

Midha Ahmad,[1] Greta Sokoloff,[1,2] and Mark S. Blumberg[1,2]
[1]Department of Psychological & Brain Sciences, University of Iowa, Iowa City, Iowa 52242 and [2]Iowa Neuroscience Institute, University of Iowa, Iowa City, Iowa 52242

The emergence of the cortical delta rhythm (1–4 Hz) during quiet sleep (QS) is a major milestone in brain development. In rats, this milestone is achieved between 8 and 12 d of postnatal (P) age. We previously reported an age-dependent increase in delta-rhythmic activity in the medullary parafacial zone (PZ) that is synchronized with cortical delta and entrained by breathing. Here, we ask whether this long-distance synchrony persists in response to perturbations to sleep homeostasis or respiration. Using male and female P12 rats, we investigated the coupling strength between the frontal cortex and PZ in response to a short but intense period of sleep deprivation. During recovery sleep, we observed similar rebounds in delta power in PZ and cortex, even in the absence of increased QS duration. Analyses of phase-locking and lagged cross-correlation revealed persistent temporal coupling between the two rhythms such that cortical delta reliably lagged PZ delta regardless of changes in sleep pressure. Curiously, we also observed an increase in the depth of breathing during recovery sleep, which we confirmed in a separate cohort of pups. Next, using moderate hypercapnia (5% CO_2) to perturb the respiratory system, we observed similar decreases in cortical and PZ delta power along with QS-dependent decreases in the depth of breathing. These findings provide additional support for the hypothesis that, at the onset of their developmental emergence, PZ and cortical delta are interconnected components of a sleep-homeostatic system that is also intimately tied with the brainstem respiratory network.

Key words: delta rhythm; development; rat; respiration; sleep; sleep deprivation

Significance Statement

We reported previously that the delta rhythm that defines quiet sleep is not confined to the forebrain but also occurs synchronously in the medulla. This study in infant rats uses two perturbations to assess the coupling strength of cortical and brainstem delta. Using sleep deprivation and hypercapnia, we show that delta power increases or decreases in lockstep in the two regions, respectively. Our results reinforce the notion that delta across these two regions is strongly coupled and adds a new dimension to our understanding of the interconnectedness of the delta rhythm and respiration.

Introduction

The cortical delta rhythm (1–4 Hz) is a signature feature of quiet sleep (QS) and among the earliest brain rhythms to develop (Frank and Heller, 1997; Jenni et al., 2004; Seelke and Blumberg, 2008). Nonetheless, it emerges rather late, ∼2–3 months of age in humans (Jenni et al., 2004) and postnatal day 12 (P12) in rats (Gramsbergen et al., 1970; Seelke and Blumberg, 2008). In adults, delta is a key indicator of sleep pressure and depth (Borbely and Achermann, 1999; Dijk, 2009) and is thought to promote learning and neural plasticity (Walker, 2009; Puentes-Mestril et al., 2019; Girardeau and Lopes-Dos-Santos, 2021). Furthermore, as a low-frequency rhythm, cortical delta enables long-range communication and nests higher-frequency activity (Buzsaki and Draguhn, 2004; Molle and Born, 2011; Buzsaki and Voroslakos, 2023). Given delta's broad functional significance, its emergence is a major developmental milestone.

To begin to understand the mechanisms influencing cortical delta's emergence in rats between P8 and P12, in a previous study (Ahmad et al., 2024), we recorded neural activity in the frontal cortex and parafacial zone (PZ), a medullary region implicated in the regulation of QS in adult rodents (Anaclet et al., 2012, 2014; Anaclet and Fuller, 2017). In that study, we predicted that an age-dependent increase in PZ activity would mirror the emergence of cortical delta. However, that is not what we found: Whereas PZ activity at P8 was arrhythmic during both QS and

Received May 11, 2026; revised July 16, 2026; accepted Aug. 17, 2026.
Author contributions: M.A., G.S., and M.S.B. designed research; M.A. performed research; M.A. and M.S.B. analyzed data; M.A., G.S., and M.S.B. wrote the paper.
This work was supported in part by a grant from the National Institute of Child Health and Human Development (R37-HD081168) to M.S.B.
The authors declare no competing financial interests.
Correspondence should be addressed to Mark S. Blumberg at mark-blumberg@uiowa.edu.
This paper contains supplemental material available at: https://doi.org/10.1523/JNEUROSCI.0802-26.2026
https://doi.org/10.1523/JNEUROSCI.0802-26.2026

active sleep (AS), by P12, we observed periods of population-level and delta-rhythmic spiking, exclusively during QS. Even more surprising, PZ's rhythmic spiking was phase-locked with a local delta rhythm (hereafter, PZ delta) and synchronized with cortical delta despite the long distance. Finally, PZ's rhythmic activity increased during the postinspiratory period, showing strong link with brainstem respiratory circuits.

Collectively, our findings suggested that the PZ and cortex function together as components of a sleep-regulatory, breathing-entrained network. Accordingly, we predicted that they would exhibit similar homeostatic responses to sleep deprivation, including parallel increases in delta power during sleep rebound (Borbely and Achermann, 1999; Tononi and Cirelli, 2006; Dijk, 2009). Here, we show that PZ and cortical delta exhibit similar rebound-related increases in delta power. The rhythms remained strongly coupled, and this coupling was not affected by sleep deprivation. Moreover, cortical delta consistently lagged PZ delta, regardless of sleep pressure. We also observed, in sleep-deprived pups, unexpected increases in the depth of breathing (i.e., respiratory amplitude) that tracked the increases in delta power. The latter finding adds a new dimension to the established links between the delta rhythm and respiration in adults (Biskamp et al., 2017; Tort et al., 2018; Karalis and Sirota, 2022). We further explored these links by exposing pups to moderate hypercapnia (5% CO_2) as a means of manipulating respiration during sleep; during QS, hypercapnia reduced respiratory amplitude while also reducing delta power in the PZ and cortex. Altogether, these findings indicate that at the time of delta's developmental emergence, homeostatic regulation is coordinated by a breathing-modulated network that spans the brainstem and forebrain.

Materials and Methods

All procedures followed the National Institutes of Health Guide for the Care and Use of Laboratory Animals (NIH Publication Number 80-23) and were approved by the Institutional Animal Care and Use Committee at the University of Iowa.

Subjects

Male and female Sprague Dawley Norway rats (*Rattus norvegicus*) were used at P12–P13 (hereafter, P12). Pups were housed in standard laboratory cages (48 × 20 × 26 cm) under a 12 h light/dark cycle, with food and water provided *ad libitum*. To control for litter effects and prevent inflated statistical power (Abbey and Howard, 1973; Lazic and Essioux, 2013), littermates were always assigned to different experimental groups. Litters were culled to eight pups by P3.

PZ and cortical activity were recorded at P12 in sleep-deprived ($n = 8$ pups, four males; body weight, 28.59 ± 0.58 g) and control ($n = 8$ pups, four males; body weight, 29.15 ± 0.91 g) rats. In a second cohort of pups, respiration was recorded using strain-gauge plethysmography in pups that experienced the sleep-deprivation protocol ($n = 7$ pups, four males; body weight, 30.08 ± 1.83 g). In a final cohort of pups, moderate hypercapnia was induced to alter respiration while PZ and cortical activity were recorded ($n = 7$ pups, three males; body weight, 29.97 ± 0.64 g).

Surgery and general experimental procedures

As described previously (Ahmad et al., 2024), on the day of testing a pup with a visible milk band was removed from the litter and anesthetized with isoflurane gas (3–5%; Phoenix Pharmaceuticals). Throughout the surgical procedure, the pup lay on a heated platform (Hallowell EMC) to maintain body temperature. The scalp was cleaned with iodine and alcohol, and a nonsteroidal anti-inflammatory drug (carprofen, 5 mg/kg; Putney) was injected subcutaneously. The scalp was removed, and a topical analgesic (0.25% bupivacaine, Pfizer, or lidocaine, Sparhawk Laboratories) was applied to the skull. The skull was then dried by applying bleach with a cotton-tipped applicator. To seal the incision and prevent bleeding, Vetbond (3M) was applied around the perimeter of the scalp incision. Two custom-made stainless-steel bipolar hook electrodes (50 µm diameter; California Fine Wire) were inserted into the left and right nuchal muscles and secured with collodion. The pup's torso was wrapped in soft surgical tape (Micropore, 3M), and, to measure respiration, a piezoelectric sensor (Unimed Electrode Supplies) was secured to the back with a surgical tape. In some experiments, respiration was measured instead using an elastic mercury-filled strain gauge (6.0–7.5 cm diameter; Hokanson), stretched around the thorax and secured with a soft tape. Finally, a stainless-steel head-fix apparatus (Neurotar) was secured to the skull using cyanoacrylate adhesive (Loctite, Henkel); the adhesive was dried rapidly using an accelerant (Insta-Set, Bob Smith Industries).

While still anesthetized, the pup was secured to a stereotaxic apparatus to complete the surgery (Stoelting). Holes were drilled in the skull to enable subsequent electrode placement in PZ (P12, +1.80 mm rostrocaudal, relative to lambda, 1.70–1.80 mm mediolateral) and the secondary motor cortex (M2; +1.0 mm rostrocaudal, relative to bregma, 1.8–2.0 mm mediolateral). A hole was also drilled over the contralateral parietal cortex for the insertion of a fine-wire thermocouple (Omega Engineering) to measure brain temperature during the acclimation period. The same hole was used for insertion of a ground/reference electrode during recording; this electrode was a chlorinated silver wire (Ag/AgCl; 0.25 mm diameter, Medwire). Mineral oil was applied to the cortical surface to prevent drying. The duration of the entire surgical procedure was ∼30 min.

After surgery, the pup was secured to a head-fix apparatus inside a grounded Faraday cage. The pup's torso was secured to an elevated narrow platform using surgical tape, with limbs dangling freely on each side. Heated water flowed through a radiator beneath the pup to provide warmth, and the local environment was humidified using moist sponges placed on top of the radiator. Brain temperature was monitored to ensure that it was stable at 36–37°C. The pup acclimated to the recording chamber for at least 1 h, and recording did not begin until regular sleep–wake cycles were observed. After acclimation, the thermocouple was replaced with the ground/reference electrode, at which time data acquisition began.

Data acquisition

Neurophysiological and respiratory data were acquired using a data acquisition system (Tucker-Davis Technologies). PZ neural data were obtained using a small-site 16-channel linear silicon electrode (A1 × 16-10mm-100-177-A16; NeuroNexus) inserted to a depth of 4.3–5.0 mm. Cortical LFPs were obtained using a large-site 16-channel linear silicon electrode (A1 × 16-10mm-100-703-A16; NeuroNexus) inserted into M2 at a depth of 0.6–1 mm. Before insertion, electrodes were coated with fluorescent DiI (Vybrant DiI Cell-Labeling Solution, Invitrogen) for subsequent histological verification. Neural signals from the electrodes were sampled at 25 kHz using a high-pass filter (0.1 Hz) and a notch filter. Piezoelectric sensor data were sampled at 30 Hz, and strain-gauge data were sampled at 1,000 Hz.

Video recording and data synchronization. As previously described (Dooley et al., 2021; Glanz et al., 2021), body and limb movements were recorded at 100 frames/s using a digital video camera (Blackfly-S; FLIR Integrated Systems). Video data were acquired using the SpinView software (FLIR). To synchronize video with electrophysiological recordings, an LED visible within the camera frame emitted a 100 ms pulse every 3 s. Following acquisition, a custom MATLAB script was used to insert blank frames in those rare instances when frames were dropped between LED pulses.

Sleep deprivation. Pups were deprived of sleep using a protocol similar to one described previously (Todd et al., 2010). Throughout the experiment, PZ and cortical activity were recorded along with respiration (using a piezoelectric sensor) and video recorded pup behavior. The experimental protocol consisted of four 30 min periods: baseline, deprivation, recovery 1 (R1), and recovery 2 (R2). The baseline period entailed uninterrupted cycling between sleep and wake. During the deprivation

period, a chilled metal spatula was gently applied to the snout around the mouth whenever cortical delta was visual observed by the experimenter, thus depriving pups of QS (but also AS as an unavoidable consequence). During R1 and R2, pups were again allowed to cycle freely between sleep and wake. Pups in the control group were left undisturbed throughout the 2 h recording period. In a follow-up experiment using a separate cohort of sleep-deprived pups, respiratory data alone were acquired using strain gauges placed around the thorax and attached to a plethysmograph (Parks Medical Electronics).

Hypercapnia. An additional cohort of P12 rats was exposed to moderate hypercapnia (5% CO_2 in air). For this experiment, respiration was measured using strain-gauge plethysmography, and PZ and cortical activities were recorded. The recording session was divided into a 30 min baseline period of normal-air breathing, a 30 min hypercapnia period, and a 30 min recovery period with normal-air breathing. During baseline and recovery periods, compressed air (21% O_2, 79% N_2) was humidified and delivered at 0.5 L/min through a tube positioned in front of the pup's snout. During the hypercapnia period, everything was the same except pups breathed air supplemented with 5% CO_2.

Histology

At the end of recording sessions, pups were killed with an intraperitoneal injection of ketamine/xylazine (10:1, >0.08 mg/kg). They were then perfused with 0.1 M phosphate-buffered saline, followed by 4% paraformaldehyde. Brains were extracted and then fixed in 4% paraformaldehyde for at least 24 h, after which they were transferred to a 30% sucrose phosphate-buffered solution for another 24–48 h before sectioning. The brain tissue was coronally sectioned at 80 μm using a freezing microtome (Leica Biosystems) and mounted on gelatin-coated slides. Electrode tracks were visualized using a fluorescence microscope system (Leica Microsystems). Slides were Nissl-stained with cresyl violet. Electrode placements were confirmed by overlaying the images of the fluorescent and Nissl-stained sections.

Data analysis

Preprocessing of neural data. Neural data were preprocessed using custom MATLAB scripts, as described previously (Dooley et al., 2021; Glanz et al., 2021; Ahmad et al., 2024). Raw LFP signals were downsampled to 1,000 Hz, smoothed with a 5 ms moving Gaussian kernel, and saved as binary files. Movements were detected in video recordings based on frame-by-frame changes in pixel intensity within regions of interest (forelimbs, hindlimbs, whole body), producing an output of real-time movement (Dooley et al., 2021; Glanz et al., 2021). Data were imported into Spike2 (Cambridge Electronic Design) or MATLAB for further analysis.

Classification of behavioral state. As described previously (Ahmad et al., 2024), behavioral state was classified using a combination of respiratory and LFP activity, limb movements, and/or nuchal EMG (Seelke and Blumberg, 2008; Isler et al., 2016; Jasmeen and Pagliardini, 2017; Dooley et al., 2021). Active wake was defined as periods when nuchal muscle tone was high and/or when multiple body parts exhibited coordinated, high-amplitude movements. As active wake transitioned to quiet wake, overt movements subsided, and muscle tone decreased. Upon the transition to QS, respiration was regular, limb movements were absent, and the amplitude of PZ and cortical delta exceeded the median LFP amplitude. AS began with the onset of limb twitching and was characterized by irregular respiration and the absence of PZ and cortical delta. If twitching ceased and at least 10 s of behavioral quiescence ensued, the AS period ended with the last twitch observed. Finally, periods of active wake, QS, and AS were required to be at least 3 s in duration to be analyzed. Microarousals (wake durations <1 s) were disregarded for the purposes of scoring changes in behavioral state.

Sleep pressure and rebound. Sleep pressure was operationalized as the total number of arousing cold-stimulus presentations during each 5-min interval of the 30-min deprivation period. The number of presentations in each interval was averaged across pups. A repeated-measures ANOVA was used to test whether the number of applications increased over time.

To detect rebounds in sleep duration, periods of wake, QS, and AS were identified as described above. The total number of bouts for each state was calculated across the three time periods (baseline, R1, and R2) and averaged across pups; these analyses were not possible during the deprivation periods themselves due to movement artifact. To determine the total time spent in each state, the cumulative bout durations of wake, QS, and AS were calculated. Repeated-measures ANOVA was used to test for changes in duration across the three periods. The total number of bouts and the average bout duration for each state were also calculated and assessed using repeated-measures ANOVA. Log-survivor plots of bout durations, pooled across pups, were generated for wake, QS, and AS during baseline, R1, and R2.

To quantify rebounds in delta power, one LFP channel was selected for analysis from each PZ and cortical electrode. Channels within the frontal cortex were selected based on their raw delta amplitude; higher-amplitude delta occurred at electrode sites located in layers 3–5. The MATLAB function, "pspectrum()," was used to generate raw power spectra. A sampling frequency of 1,000 Hz was used, and power-spectral values between 1 and 30 Hz were calculated. Power-spectral values were normalized to peak delta power, at 1.5–2.5 Hz, during baseline; normalized power was then averaged across pups. Finally, the area under the power-spectral curve within delta frequencies was calculated for each pup to compare delta power differences across the three periods. As a multiway ANOVA (three levels within, two levels between) failed Levene's test for equality of variances, one-way repeated-measures ANOVAs were instead used to test for changes in PZ and cortical delta power across time.

Quantifying PZ–cortical coupling for individual delta waves. In sleep-deprived adult rats, the prevalence of high-amplitude delta waves increases during recovery sleep (Vyazovskiy et al., 2007). To assess this phenomenon in sleep-deprived P12 rats, we extracted the peak amplitudes of individual delta waves in the PZ and cortex using custom MATLAB scripts. To do this, LFP signals were bandpass filtered (1–4 Hz) to isolate delta waves, the peak of each wave was identified, and frequency distributions of peak amplitudes in the PZ and cortex for each pup during baseline, R1, and R2 were constructed. For each pup's frequency distribution of PZ and cortical delta during baseline, values exceeding three standard deviations above and below the mean were excluded from further analysis. From the resulting baseline distributions of delta amplitude, four percentile ranges were defined: 20th–40th, 40th–60th, 60th–80th, and ≥80th. These ranges served as thresholds to categorize the amplitude of individual delta waves, with waves exceeding the 80th percentile designated as high amplitude. For the baseline, R1, and R2 periods, the proportion of delta peaks falling within each percentile range was computed relative to the total number of detected delta peaks.

Perievent time histograms (PETHs) were generated to measure the degree to which high-amplitude delta peaks in the PZ and cortex co-occurred during the recovery periods. For each individual cortical delta wave, the time of peak amplitude was used as the trigger, and PZ delta amplitude was plotted in relation to the trigger (window, 1 s; offset, 0.5 s; bin size, 100 ms). The PETHs for each pup were normalized to the maximum value within the window and then averaged across pups.

To test whether the co-occurrence of high-amplitude peaks in the PZ and cortex occurred above chance levels, a Monte Carlo approach was employed. Specifically, the sequence of interpeak intervals in the cortical delta signal was shuffled 1,000 times to randomize trigger times while preserving the original lengths of the intervals. (The PZ delta record was not manipulated.) Each shuffled train of cortical peaks was then jittered to remove any residual temporal alignment between signals, ensuring that any detected co-occurrence was not driven by edge effects; the value of the jitter was derived from the median interpeak interval. The width at half-height of the average PETH for unshuffled data defined the temporal window used to calculate the probability of co-occurrence. This window was first applied to the unshuffled data to compute the observed probability and then to each of the 1,000 shuffled datasets to

compute the probability expected by chance. Expected probabilities were averaged within each pup, and observed versus expected probabilities were compared across baseline, R1, and R2 periods using a 3 (period) × 2 (observed vs expected) repeated-measures ANOVA.

Quantifying phase connectivity and directionality between PZ and cortical delta. Phase relations between PZ and cortical LFPs in the delta range during QS were quantified using phase differences and phase-locking values (PLVs). LFPs were first bandpass filtered in the delta range (1–4 Hz), and the Hilbert transform was applied to extract the instantaneous phase of each signal. Phase differences (cortex − PZ) were computed at each time point and summarized as normalized histograms (bin size, 12°; probabilities sum to 1) and visualized as rose plots. PLV was calculated as the absolute value of the mean phase difference (expressed as a complex vector) between the two signals. For each pup, nonuniformity of phase differences was assessed using Rayleigh's test. Group differences in PLV between sleep-deprived ($n = 8$) and control ($n = 8$) pups were evaluated using an independent-samples Mann–Whitney U test.

To obtain a measure of directionality, lagged cross-correlations were computed as previously described (Adhikari et al., 2010). Briefly, using the bandpass filtered (1–4 Hz) LFPs, instantaneous amplitude during QS was computed using the Hilbert transform. The lagged cross-correlations between PZ and cortical amplitudes were calculated using the "xcorr" MATLAB function. For each pup, the lag corresponding to the peak cross-correlation was extracted. Group-level cross-correlation values were averaged, and the distribution of peak lags was plotted across animals. Peak lags were tested against zero using a Wilcoxon matched-pair signed-rank test in the sleep-deprived group and a one-sample t test in controls. We then repeated this analysis in the sleep-deprived group to test if sleep pressure selectively alters directionality. For baseline, R1, and R2 periods, peak lags values were tested using a Friedman test.

Quantifying changes in depth and frequency of breathing during sleep deprivation and hypercapnia. For measures of respiratory amplitude, strain-gauge plethysmography provides a more direct measure than piezoelectric sensors. Thus, in a separate cohort of pups, we repeated the sleep-deprivation experiment using strain-gauge plethysmography. Respiratory amplitude of each breath was measured as the absolute difference between peak and trough values. Next, for each 30-min recording period (baseline, R1, and R2), the root mean square (RMS) of the respiratory amplitude was calculated from all respiratory amplitudes measured during wake, QS, and AS during each period. Changes in RMS (hereafter, respiratory amplitude) during R1 and R2 were assessed using a one-sample t test against a hypothesized value of 1 (i.e., normalized baseline) or, if normality assumptions were violated, a Wilcoxon matched-pair signed-rank test. This analysis was also used for the hypercapnia experiment. Additionally, respiratory frequency was quantified by detecting peaks in the respiratory rhythm and counting the total number of peaks during the baseline, hypercapnia, and recovery periods across sleep–wake states. For each period and state, the total number of peaks was divided by the total duration of that state to obtain respiratory frequency. These values were normalized to baseline, and a one-sample t test or Wilcoxon signed-rank test was used as described above.

Quantifying ventilation during hypercapnia. To quantify changes in ventilation before and after CO_2 exposure, normalized respiratory frequency and normalized respiratory amplitude, calculated as described above, were multiplied to generate normalized ventilation values for each behavioral state. Because both respiratory frequency and amplitude were normalized to the corresponding baseline values, the resulting ventilation values were also normalized such that baseline equaled 1. Separate one-sample t tests (or Wilcoxon signed-rank tests when normality assumptions were not met) were used to determine whether normalized ventilation during hypercapnia differed from the baseline reference value of 1 for wake, QS, and AS. Hypercapnia and recovery values were then compared within each behavioral state using paired t tests (or Wilcoxon signed-rank tests when appropriate).

Quantifying changes in sleep–wake architecture during hypercapnia. Similar to the sleep-deprivation experiment, the total number of wake, QS, and AS bouts was calculated across three time periods (baseline, hypercapnia, and recovery) and averaged across pups. The average and cumulative durations of wake, QS, and AS were calculated for each time period. Repeated-measures ANOVA was used to test for changes in cumulative duration across the three periods. The total number of bouts and the average bout duration for each state were also calculated and tested using repeated-measures ANOVA.

Statistical analysis

All statistical analyses were conducted using SPSS 29 (IBM) or MATLAB. Statistical tests included repeated-measures ANOVA, paired t tests, and one-sample t tests. Data were tested for normality using the Shapiro–Wilk test. When normality assumptions were violated, nonparametric tests were used. When appropriate, Mauchly's test was used to test for sphericity. In analyses where sphericity was violated, a Huynh–Feldt correction was applied to the degrees of freedom. Bonferroni's corrections were used when appropriate to adjust alpha for multiple comparisons. The measure of effect size was partial eta-squared adjusted for positive bias (Mordkoff, 2019) for ANOVAs, Hedges' g for t tests, and r values for Wilcoxon tests (Peres, 2025). Unless otherwise stated, means are always presented with their standard error (SEM).

Data exclusion was rare. One value that was 3 SDs above the mean was excluded as an outlier, and one pup was excluded due to persistent wakefulness.

Results

We recorded neural activity in the frontal cortex and PZ in unanesthetized, head-fixed P12 rats as they cycled between sleep and wake (Fig. 1*A–C*). Our first goal was to determine whether sleep deprivation causes parallel effects on delta power in the two structures during recovery sleep. In a separate experiment, we manipulated respiration using moderate hypercapnia to further assess the strength of coupling between the cortex and PZ.

Deprived P12 rats do not exhibit sleep rebound in QS duration

In the sleep-deprived group ($n = 8$ pups), neural activity and behavior were recorded continuously over 2 h, evenly divided into baseline, sleep deprivation, R1, and R2 periods (Fig. 1*D*). Sleep deprivation was achieved by applying a cold stimulus to the snout whenever the experimenter detected cortical delta. The number of stimulations required to maintain wakefulness increased significantly across the deprivation period ($F_{(5,35)} = 18.04$; $p < 1 \times 10^{-7}$; adj. $\eta p^2 = 0.68$), demonstrating a monotonic accumulation of sleep pressure (Fig. 1*E*). The number of stimulations applied in the last 5 min of the period was twice the number during the first 5 min ($t_{(7)} = 7.32$; $p = 0.00016$; Hedges' $g = 1.33$).

Because the sleep cycle of P12 rats progresses sequentially from QS to AS (Seelke and Blumberg, 2008), any deprivation procedure that targets QS-related delta also necessarily deprives pups of AS. Thus, we did not expect sleep rebound to be specific to QS. Indeed, mean QS duration was unchanged during the recovery periods; instead, AS duration increased, and wake duration decreased during recovery sleep (Fig. 1*F*). Repeated-measures ANOVA revealed significant main effects of state ($F_{(2,14)} = 14.42$; $p = 0.0004$; adj. $\eta p^2 = 0.63$) and time ($F_{(2,14)} = 10.48$; $p = 0.0017$; adj. $\eta p^2 = 0.54$), as well as a significant state × time interaction ($F_{(4,28)} = 4.43$; $p = 0.0067$; adj. $\eta p^2 = 0.30$). The significant decrease in total wake duration during R1 indicates that total sleep duration increased, irrespective of the lack of selective rebounds in mean QS and AS durations during R1; indeed, there was a significant increase in total sleep duration

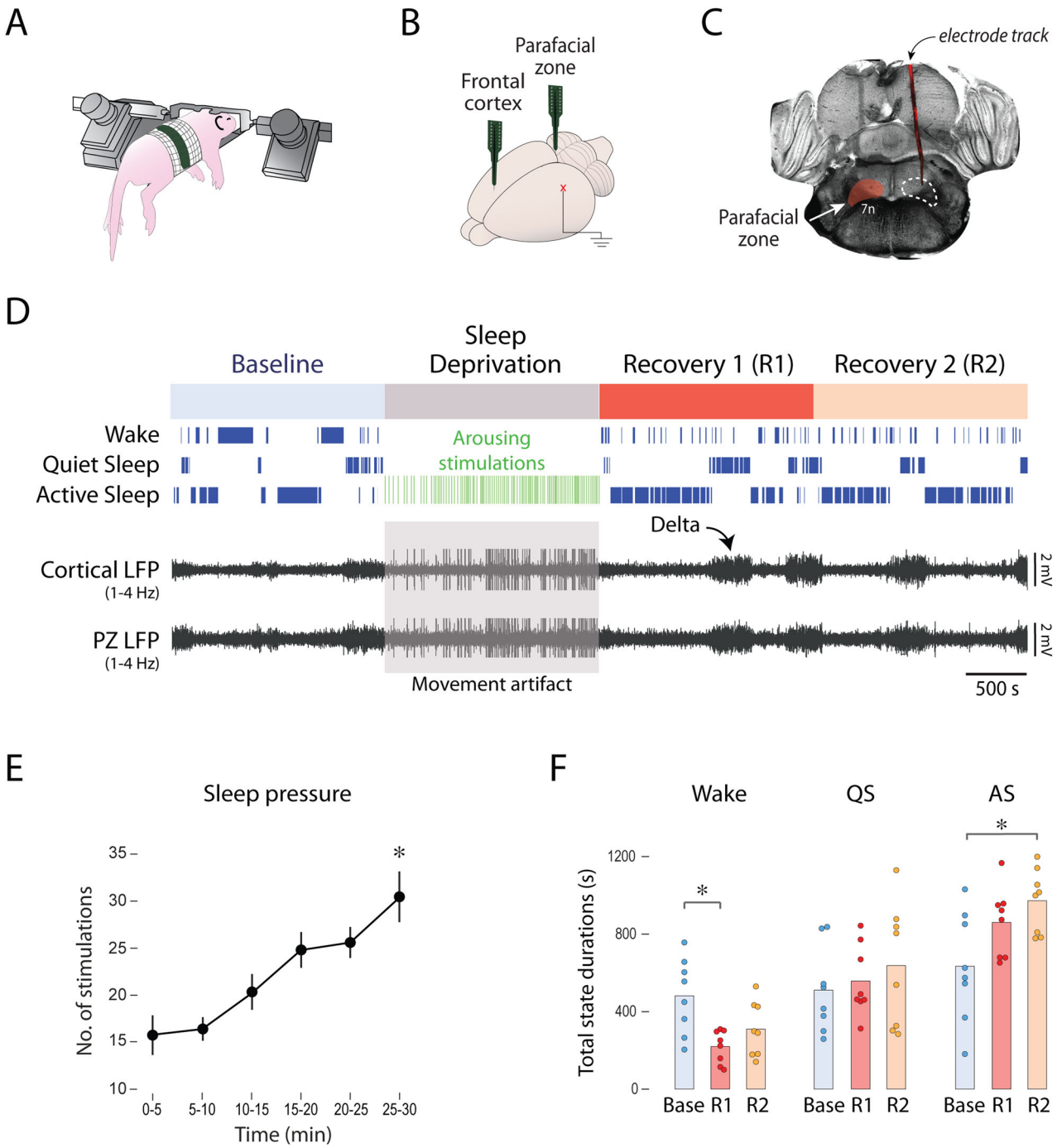

Figure 1. Sleep deprivation in P12 rats. ***A***, Sleep–wake behavior and neural activity were recorded from head-fixed pups. ***B***, Silicon electrodes were inserted into the frontal cortex and ipsilateral PZ. ***C***, Histological confirmation of a representative electrode placement in PZ. ***D***, Representative data from one pup in the sleep-deprivation group. The 30 min baseline (Base), deprivation, Recovery 1 (R1), and Recovery 2 (R2) periods are shown; the color codes for each period are used throughout the figures. From top: Bouts of wake, QS, and AS, and cortical and PZ local field potentials (LFPs) filtered at delta frequencies (1–4 Hz). For the sleep-deprivation period, the arousing stimulations are represented as vertical green lines; the gray box indicates that the LFP data are corrupted by movement artifact. ***E***, The number of arousing stimuli presented over time during the sleep-deprivation period, indicative of accumulating sleep pressure. $n = 8$ pups. The asterisk denotes significant difference from the first period; $p < 0.001$. ***F***, Mean total state durations for wake, QS, and AS for the baseline, R1, and R2 periods. Asterisks denote significant differences between groups; $ps < 0.01$.

during recovery ($F_{(2,14)} = 13.86$; $p = 0.0005$; adj. $\eta p^2 = 0.62$; data not shown). This result is consistent with the fact that the sleep-deprivation protocol, by targeting QS, necessarily deprives pups of both QS and AS.

Next, we assessed separately the mean number of bouts and the mean duration of each bout because those two variables, when multiplied, determine the mean total state duration. We found that the increase in total AS duration and decrease in total wake duration during recovery sleep were due primarily to an increase in the number of AS bouts and shorter mean wake durations (Fig. S1*A*,*B*). Again, QS remained unchanged across these measures.

To provide a more sensitive assessment of the statistical structure of the sleep-bout data, we constructed log-survivor plots of

wake-, QS-, and AS-bout durations, pooled within baseline, R1, and R2 periods (Fig. S1). These plots show that the longest QS bouts were more consolidated during recovery sleep, thus providing evidence of an emerging selective effect of sleep deprivation on QS bout durations. In contrast, wake-bout durations were more fragmented during recovery sleep while AS-bout durations were unchanged.

Recordings for the control group ($n = 8$ pups) followed the same timeline, but the pups were undisturbed during the second 30 min period (Fig. S2*A*). As expected, control animals exhibited no significant changes in total state durations ($F_{(4,28)} = 0.80$), number of bouts ($F_{(4,28)} = 2.6$), or mean bout durations ($F_{(4,28)} = 0.19$; Fig. S2*B–D*).

In summary, the strongest effects of sleep deprivation on sleep architecture at P12 entailed decreases in mean wake durations during R1, indicative of increases in sleep durations. In contrast, the evidence for selective rebounds in QS and AS bouts or durations during R1 was relatively weak or absent.

Sleep-deprived pups exhibit parallel rebounds in cortical and PZ delta power

Sleep deprivation had a substantial impact on delta rebound (Fig. 2*A*, left). Specifically, mean power spectra for cortical and PZ delta revealed ~35% increases in power during R1, with power decreasing back toward baseline levels during R2. Mean power spectra for the control group did not differ across periods (Fig. 2*A*, right).

In the sleep-deprived group, there was a significant effect of time on delta power in both regions (cortex, $F_{(1.13,9.18)} = 5.03$; $p = 0.04$; adj. $\eta p^2 = 0.34$; PZ, $F_{(2,14)} = 6.05$; $p = 0.013$; adj. $\eta p^2 = 0.39$; Fig. 2*B*, left), with mean delta power during R1 being significantly greater than baseline in both the cortex ($t_{(7)} = 3.13$; $p = 0.016$; adj. $\alpha = 0.017$; Hedges' $g = 1.20$) and PZ ($t_{(7)} = 4.085$; $p = 0.005$; adj. $\alpha = 0.017$; Hedges' $g = 1.26$). In contrast, during R2, mean delta power did not differ significantly from baseline in either region. In the control group, although the small changes in cortical delta power across testing periods were nonetheless significant ($F_{(2,14)} = 7.52$; $p = 0.006$), post hoc tests were not (Fig. 2*B*, right); there was no significant change in PZ delta power across time ($F_{(1.3,9.2)} = 2.23$).

Sleep-deprived pups exhibit increased high-amplitude delta waves in the PZ and cortex during recovery sleep

In sleep-deprived adult rats, recovery sleep is characterized by the increased expression of individual high-amplitude delta waves that contribute to increases in delta power (Vyazovskiy et al., 2007). We observed a similar pattern in sleep-deprived P12 rats, with recovery sleep marked by the increased expression of high-amplitude delta waves. In both cortical and PZ LFPs, this phenomenon was expressed as parallel fluctuations in the instantaneous power envelopes (Fig. 3*A*).

To quantify this effect, we first identified the peaks of individual delta waves and classified them according to their amplitudes, relative to each pup's baseline (Fig. 3*B*; see Materials and

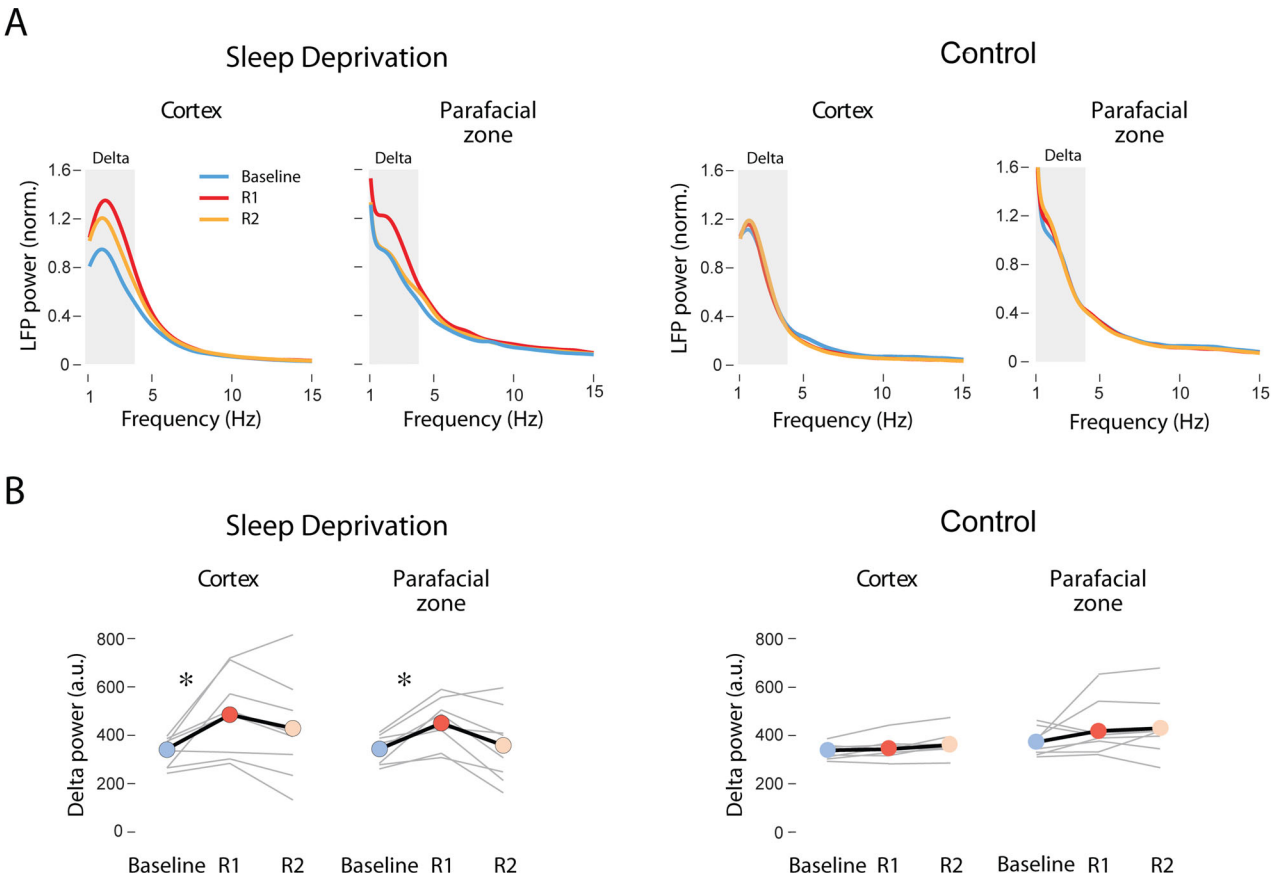

Figure 2. Sleep-deprived P12 rats exhibit delta power rebound in the cortex and PZ. ***A***, Mean power spectra for the frontal cortex and PZ during QS for baseline, R1, and R2 periods for the sleep-deprivation (left) and control (right) groups. Gray boxes indicate delta frequencies (1–4 Hz). Delta power was normalized to peak power (between 1.5 and 2.5 Hz) during baseline and then averaged across pups. ***B***, Mean delta power (black lines; in arbitrary units, a.u.) during QS across time for the sleep-deprivation (left) and control (right) groups. Gray lines show data for individual pups. Asterisks denote significant differences between time periods; *p*s < 0.02.

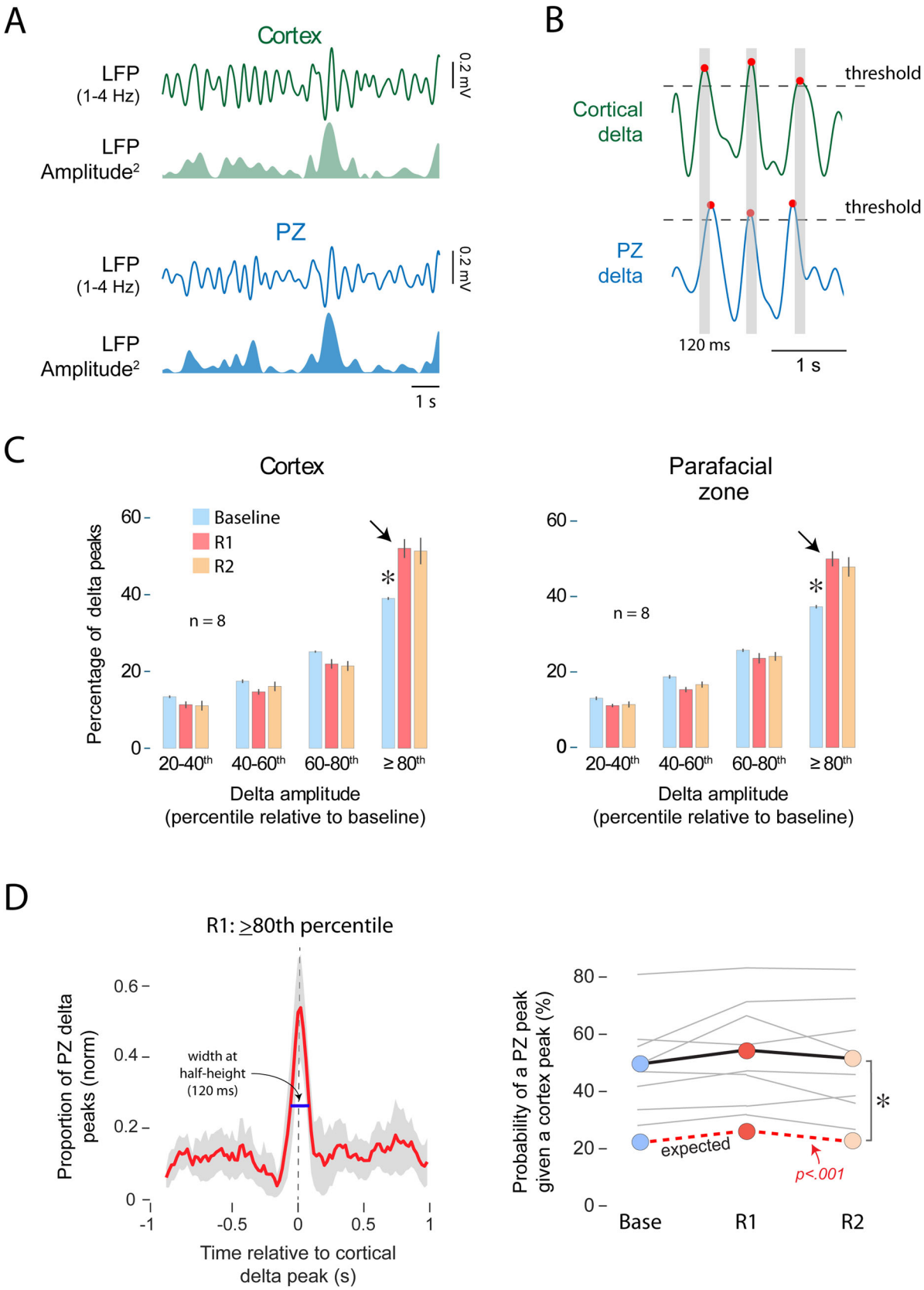

Figure 3. Sleep deprivation in P12 rats causes parallel increases in high-amplitude delta waves in the cortex and PZ. ***A***, Representative data from one pup during QS showing instantaneous power in the PZ and cortex during recovery sleep (R1). From top, Cortical LFP filtered at delta frequencies, squared instantaneous amplitude of cortical delta, PZ LFP filtered at delta frequencies, squared instantaneous amplitude of PZ delta. ***B***, Representative 2 s periods showing the co-occurrence of high-amplitude delta waves in the cortex (top) and PZ (bottom). Gray boxes indicate 120 ms time windows centered on peak cortical delta. ***C***, Frequency distributions of delta peaks that fell within defined threshold ranges in the cortex (left) and PZ (right) for baseline, R1, and R2 periods. Asterisks denote significant difference from other two time periods; *p*s < 0.01. ***D***, Left, Mean perievent histogram for PZ delta peaks triggered on cortical delta peaks. The width at

Methods). This analysis confirmed a marked shift toward higher-amplitude waves during recovery sleep in both brain regions (Fig. 3C). Repeated-measures ANOVA for each brain area separately revealed significant main effects of amplitude (cortex, $F_{(3,21)} = 153.93$; $p < 1 \times 10^{-7}$; adj. $\eta p^2 = 0.95$; PZ, $F_{(3,21} = 211.79$; $p < 1 \times 10^{-7}$; adj. $\eta p^2 = 0.96$) and time (cortex, $F_{(2,14)} = 169.90$; $p < 1 \times 10^{-7}$; adj. $\eta p^2 = 0.96$; PZ: $F_{(2,14)} = 63.99$; $p < 1 \times 10^{-7}$; adj. $\eta p^2 = 0.89$), as well as significant amplitude × time interactions (cortex, $F_{(6,42} = 10.85$; $p < 1 \times 10^{-7}$; adj. $\eta p^2 = 0.55$; PZ, $F_{(6,42)} = 13.73$; $p < 1 \times 10^{-7}$; adj. $\eta p^2 = 0.61$). Consistent with the findings in adult rats (Vyazovskiy et al., 2007), the highest-amplitude delta waves (i.e., those above the 80th percentile) were significantly more prevalent during recovery sleep in both the cortex ($F_{(2,14)} = 14.15$; $p = 0.0004$; adj. $\eta p^2 = 0.62$) and PZ ($F_{(2,14)} = 20.26$; $p = 0.00007$; adj. $\eta p^2 = 0.71$).

We next determined whether the highest-amplitude waves are temporally coupled in the two brain regions. For this analysis, we constructed perievent histograms of PZ delta peaks triggered on cortical delta peaks during R1. This analysis revealed a distinct peak at 0 s, indicating tight temporal coupling (Fig. 3D, left); ~60% of PZ peaks occurred within 120 ms of cortical peaks, corresponding to nearly one-quarter of a 2 Hz delta cycle. This level of co-occurrence was significantly greater than expected by chance ($F_{(1,7)} = 22.32$; $p = 0.002$; adj. $\eta p^2 = 0.73$; Fig. 3D, right). The same analysis during R2 yielded a similar result (data not shown).

Importantly, this coupling did not vary across time, with no significant main effect of time ($F_{(2,14)} = 3.11$) or a significant interaction ($F_{(2,14)} = 0.78$). Thus, sleep deprivation increases the occurrence of high-amplitude delta waves without altering coupling between the two structures.

The cortex lags PZ in the delta-frequency range

Because high-amplitude delta waves in the PZ and cortex were heterogeneous and were tightly coupled before and after sleep deprivation, we next asked whether this coupling entails a consistent phase relation between the two rhythms. First, we computed the mean phase differences between PZ and cortical delta during QS for the sleep-deprived and control groups (Fig. 4A). In both groups, phase differences were nonzero and clustered; there was a consistent phase difference (cortex − PZ) between the two rhythms of 5–30°. To assess the strength of this coupling, we computed PLVs for the two LFPs (Fig. 4B). PLVs were first tested for nonuniformity using Rayleigh's test; all PLVs were significant ($ps < 1 \times 10^{-5}$). Next, we tested for differences in PLVs between the sleep-deprived and control groups. PLVs for the sleep-deprived and control groups were not significantly different ($Z = 1.68$; $p = 0.11$), indicating again that the two delta rhythms are strongly coupled and that this coupling is not affected by sleep deprivation.

Thus, these findings replicate those from our previous study (Ahmad et al., 2024) in demonstrating coherent PZ and cortical delta. We next assessed the direction of information flow by computing the cross-correlations of the instantaneous amplitudes of the two delta rhythms during QS (Adhikari et al., 2010). Peak cortical delta amplitude consistently lagged PZ delta amplitude by an average of ~28 ms (sleep-deprived group) and ~23 ms (control group; Fig. 4C). Peak lags for all individual pups had positive values and were significantly different from zero for the sleep-deprived ($Z = 2.52$; $p = 0.012$; $r = 0.89$) and control ($t_{(7)} = 6.29$; $p = 0.003$; Hedges' $g = 2.26$) groups (Fig. 4D). Finally, peak lags were consistently positive at all three testing periods (Fig. 4E), with no significant changes over time ($\chi^2_{(2)} = 1.87$; $p = 0.39$; Fig. 4F).

Pups increase their depth of breathing during recovery sleep

In the previous experiment, it appeared that pups increased their depth of breathing during recovery sleep. Because the piezoelectric sensor used to measure breathing does not provide a direct measure of respiratory amplitude, we repeated the sleep-deprivation protocol in a new cohort of pups ($n = 7$) but using strain-gauge plethysmography (Fig. 5). Respiratory amplitude during QS increased significantly during R1, ~30% over baseline values ($t_{(6)} = 3.56$; $p = 0.012$; Hedges' $g = 2.06$). During R2, amplitude was lower than during R1 and not significantly different from baseline ($t_{(6)} = 1.704$; $p = 0.15$). Thus, increased respiratory amplitude is a reliable feature of recovery sleep at this age, mirroring the observed increase in delta power in the previous experiment.

Hypercapnia suppresses PZ and cortical delta power and respiratory amplitude

As a second test of the functional coupling between PZ and cortical delta and their relationship to respiration, we turned to a manipulation that specifically targets the respiratory system. Hypercapnia, an increase in carbon dioxide in the blood, can be produced by breathing air supplemented with CO_2. Moderate hypercapnia has variable effects on the respiratory rate and amplitude in infant rats (Saetta and Mortola, 1985; Abu-Shaweesh et al., 1999; Wickstrom et al., 2002; Putnam et al., 2005; Steggerda et al., 2010), depending on such factors as age, behavioral state, duration of exposure, and anesthesia. Because sleep has not been explicitly monitored during hypercapnia in infant rats of any age, it was difficult to predict how hypercapnia would affect breathing. However, given the findings above, we predicted that regardless of whether hypercapnia increased or decreased breathing amplitude, we would see parallel changes in PZ and cortical delta power.

In P12 rats ($n = 7$ pups), we assessed the effect of moderate hypercapnia on respiration and PZ and cortical delta power. Pups breathed normal air for 30 min, followed by 30 min of hypercapnia, and finally a return to normal air for 30 min (Fig. 6A). Hypercapnia produced immediate arousal lasting 2.5–10.8 min (mean = 5.6 ± 2.8 min), after which time pups entered QS and thereafter cycled between sleep and wakefulness. We quantified the effects of hypercapnia on sleep–wake architecture across the 30-min period and, even including the initial arousal period, found no significant changes in total state duration (Fig. S3A; $F_{(4,24)} = 2.12$), number of bouts (Fig. S3B; $F_{(4,24)} = 1.90$), or average bout duration (Fig. S3A; $F_{(4,24)} = 0.70$).

Even though hypercapnia did not significantly alter sleep architecture, it did suppress cortical and PZ delta power during QS by ~38% (Fig. 6B). In both brain regions, the decreases in delta power were reversed in the recovery period upon restoration of normal air. Statistical analysis revealed a significant

←

half-height (120 ms) defines time windows for calculating the probability that cortical and PZ peaks co-occurred. Right, Mean observed probability (black line) of a PZ high-amplitude peak given a cortex high-amplitude peak. Gray lines show probabilities for individual pups. Red dotted line is the mean expected probability, calculated from shuffled data. Asterisk denotes significant difference between expected and observed probability; $p < 0.01$.

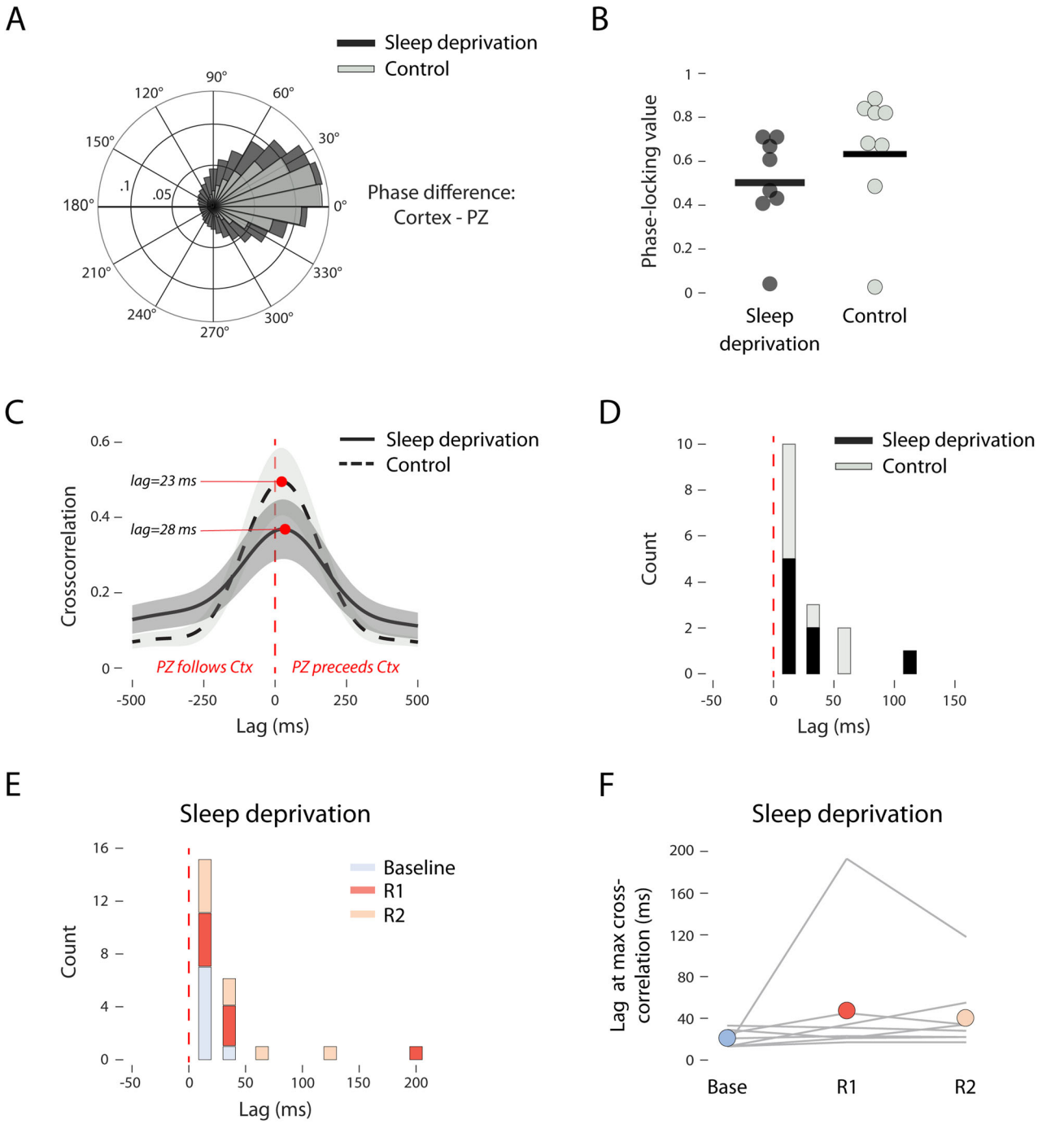

Figure 4. Cortical delta consistently lags PZ delta in P12 rats. ***A***, Mean phase difference between cortical and PZ delta for the sleep-deprivation and control groups. $n = 8$/group. ***B***, Mean PLVs for cortical and PZ delta for the sleep-deprivation and control groups. Individual pups are shown, all of which exhibited significant nonuniformity (Rayleigh's test; $ps < 1 \times 10^{-5}$). ***C***, Mean lagged cross-correlations of instantaneous amplitudes for cortical and PZ delta for the sleep-deprivation and control groups. Mean lags at the maximum cross-correlations are indicated by red dots. ***D***, Count distribution of lags at maximum cross-correlation for each individual pup in the sleep-deprived and control groups. ***E***, Count distribution of lags at maximum cross-correlation for the sleep-deprivation group for the baseline, R1, and R2 periods. ***F***, Mean lags at maximum cross-correlation across time periods for the sleep-deprivation group. Gray lines represent data for individual pups.

effect of time on cortical ($F_{(1.08,6.48)} = 9.83$; $p = 0.017$; adj. $\eta p^2 = 0.56$) and PZ ($F_{(2,12)} = 6.94$; $p = 0.01$; adj. $\eta p^2 = 0.43$) delta power, with mean delta power during hypercapnia being significantly lower than baseline in both the cortex ($t_{(6)} = 12.10$; $p = 0.00002$; adj. $\alpha = 0.017$; Hedges' $g = 3.31$) and PZ ($t_{(6)} = 6.2$; $p = 0.0008$; adj. $\alpha = 0.017$; Hedges' $g = 2.65$).

As predicted, the decreases in delta power were mirrored by a nearly 40% decrease in respiratory amplitude during the hypercapnia period (Fig. 7*A*). Compared with baseline, the reduction in respiratory amplitude was significant during the hypercapnia period ($t_{(6)} = 3.79$; $p = 0.009$; Hedges' $g = 2.03$), but not during recovery ($t = 1.67$; $p = 0.15$). The effect of hypercapnia on respiratory amplitude was specific to QS: Hypercapnia did not significantly alter respiratory amplitude during either wake or AS ($ps < 0.96$; Fig. S4*A*). Finally, to directly compare hypercapnia-induced changes in peak PZ and cortical delta in relation to

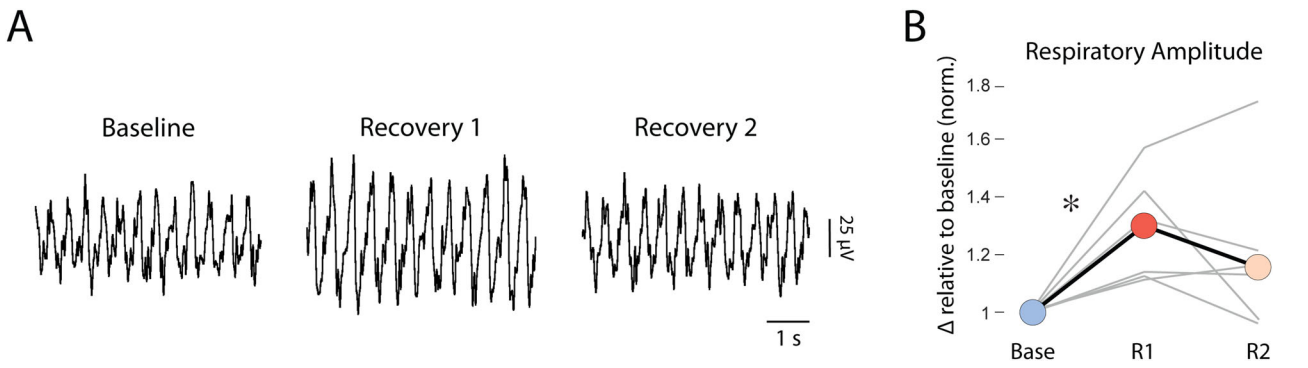

Figure 5. Respiratory amplitude increases during recovery sleep in P12 rats. ***A***, Representative data from one pup showing respiratory amplitude changes across time during QS. ***B***, Mean respiratory amplitude across time (black line), normalized to baseline. Gray lines represent data from individual pups. Asterisk denotes significance difference between the two time periods; $p < 0.05$.

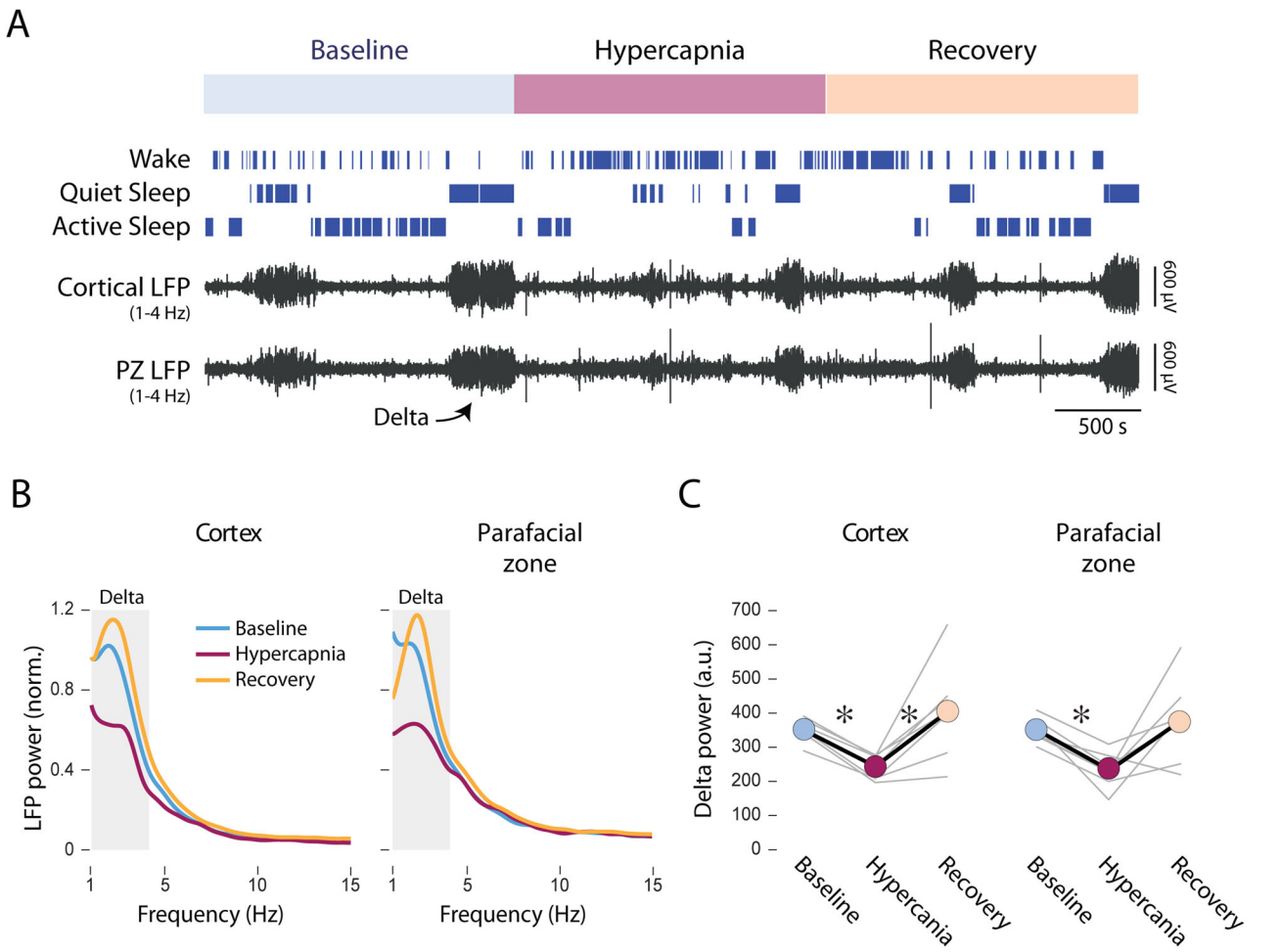

Figure 6. Hypercapnia suppresses QS-related cortical and PZ delta power in P12 rats. ***A***, Representative recording in a pup cycling through sleep and wakefulness. The 30 min baseline, hypercapnia (5% CO_2), and recovery periods are shown; the same color codes for each period are used throughout. From top, Bouts of wake, QS, and AS, and cortical and PZ LFPs filtered at delta frequencies (1–4 Hz). ***B***, Mean power spectra for cortex (left) and PZ (right) during baseline, hypercapnia, and recovery periods. $n = 7$ pups. Gray boxes indicate delta frequencies (1–4 Hz). Delta power was normalized to peak power (between 1.5 and 2.5 Hz) during baseline and then averaged across pups. ***C***, Mean power (black lines; arbitrary units, a.u.) within delta frequencies during QS for the baseline, hypercapnia, and recovery periods. Gray lines show data for individual pups. Asterisks indicate significant differences between time periods; $p < 0.01$.

peak respiratory amplitude, we plotted them against each other. All pups exhibited parallel decreases in delta and respiratory amplitude in both brain structures (shaded values in Fig. 7*B*). In contrast, upon restoration of normal air, respiratory amplitudes were more variable and did not immediately return to baseline, perhaps reflecting a delay in clearing CO_2 from the blood.

In contrast to respiratory amplitude, hypercapnia produced, on average, 30–35% increases in respiratory frequency that were not state-dependent (Fig. 7*C*; Fig. S4*B*). The increases during QS ($t_{(6)} = 5.28$; $p = 0.002$; Hedges' $g = 2.85$), wake ($Z = 2.37$; $p = 0.018$; $r = 0.89$), and AS ($t_{(6)} = 25.23$; $p < 1 \times 10^{-6}$; Hedges' $g = 13.48$) were all significant (Fig. 7*C*; Fig. S4*B*). The decreases

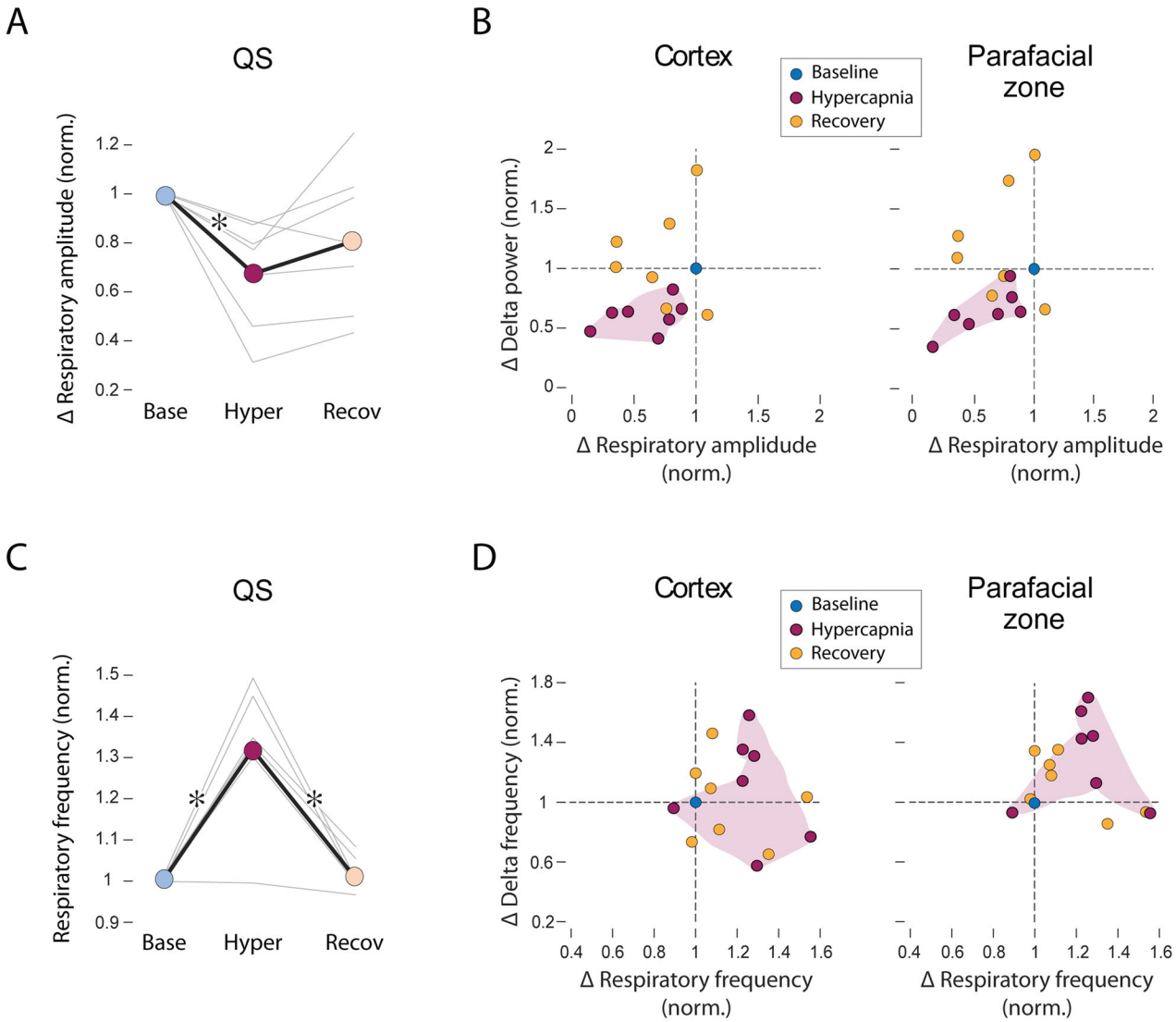

Figure 7. Hypercapnia evokes parallel decreases in QS-related respiratory amplitude and delta power but increases in respiratory frequency. ***A***, Mean change in respiratory amplitude (black line) across time, normalized to baseline values. Gray lines represent changes for individual pups. $n = 7$. Asterisk denotes significant difference between time periods; $p < 0.01$. ***B***, Changes in peak delta power in the cortex (left) and PZ (right) plotted against changes in peak respiratory amplitude (all normalized to baseline). Each dot represents an individual pup. The shaded area denotes distribution of values during hypercapnia. ***C***, ***D***, Same as in ***B*** and ***C*** but for respiratory frequency.

in respiratory frequency during the recovery period were also significant for QS ($t_{(6)} = 5.31$; $p = 0.002$; Hedges' $g = 0.97$), wake ($Z = -2.37$; $p = 0.018$; $r = 0.89$), and AS ($t_{(6)} = 14.79$; $p = 6 \times 10^{-6}$; Hedges' $g = 7.13$). Plots for individual pups show a tendency toward increased delta and respiratory frequencies during hypercapnia (Fig. 7*D*, shaded values) and a variable return toward baseline during the recovery period.

Finally, to assess the overall ventilatory response to hypercapnia, we quantified minute ventilation as the product of respiratory frequency and amplitude (Fig. S4*C*). Because respiratory frequency increased similarly across all three states, state-dependent differences in respiratory amplitude determined ventilation. Accordingly, during wake and AS, ventilation increased ~80 and 60% above baseline, respectively; these increases were significant (wake, $Z = 2.37$; $p = 0.018$; $r = 0.90$; AS, $t_{(6)} = 3.63$; $p = 0.015$; Hedges' $g = 1.79$). In contrast, there was a small but nonsignificant decrease in ventilation during QS ($Z = -1.10$; $p = 0.31$). During the recovery period, ventilation during wake and AS decreased significantly back toward baseline levels (wake, $Z = -2.37$; $p = 0.018$; $r = 0.90$; AS, $t_{(6)} = 4.19$; $p = 0.006$; Hedges' $g = 1.43$). Together, these findings indicate that pups mounted an appropriate ventilatory response to hypercapnia, but this response was modulated by behavioral state and was specifically absent during QS.

In summary, hypercapnia induced collective effects on PZ and cortical delta power and respiratory amplitude that were opposite to those observed during recovery sleep after sleep deprivation. That the depressive effect of hypercapnia on respiratory amplitude occurred selectively during QS reinforces the notion that delta power and respiratory amplitude are mechanistically related.

Discussion

The present study identifies coordinated, state-dependent responses in P12 rats linking PZ and cortical delta with respiratory dynamics. First, sleep deprivation elicited parallel increases in PZ and cortical delta power during recovery sleep. Second, this rebound involved recruitment of high-amplitude delta waves in both structures, along with high-amplitude breathing. Third, PZ and cortical delta were strongly phase-locked, with cortical

delta consistently lagging PZ delta. Finally, hypercapnia induced parallel decreases in PZ and cortical delta power along with state-dependent decreases in breathing amplitude. Thus, the synchronization of PZ and cortical delta that we reported previously at this age (Ahmad et al., 2024) persists in the face of two distinct perturbations, supporting the notion that PZ and cortical delta are coupled components of a homeostatically regulated delta-generating system. Our findings further implicate respiration as a functionally integrated element of this system at the time of delta's developmental onset.

Delta power rebound occurs as early as P12

In adult mammals, QS-related sleep homeostasis is expressed during recovery sleep as increases in delta power and/or sleep duration (Borbely and Achermann, 1999; Leemburg et al., 2010; Allada et al., 2017). In a previous study of infant rats, compensatory increases in sleep duration occurred at P12, whereas delta power rebound was not observed until P24 (Frank et al., 1998). One explanation for the discrepant findings may lie in the different methods used for sleep-depriving pups. The efficacy of our method was first demonstrated in rats at P2 and P8, prior to the developmental emergence of cortical delta (Todd et al., 2010). Here, at P12, this method also proved effective for rapidly generating intense sleep pressure and revealing the capacity for delta homeostasis.

Sleep deprivation does not disrupt the coupling between PZ and cortical delta

In adult rats, sleep deprivation increases the incidence of high-amplitude, synchronized slow waves during recovery sleep (Vyazovskiy et al., 2007; Nir et al., 2011). Similarly, PZ and cortical delta rebound in the present study was driven by the selective recruitment of high-amplitude delta waves. Critically, these waves were coupled in PZ and cortex, suggesting the action of a shared homeostatic network that augments delta power without disrupting delta synchrony. Supporting this interpretation, the synchronization between PZ and cortical delta remained high, with consistent, nonzero phase relationships that were unaffected by sleep deprivation. Also, cortical delta consistently lagged PZ delta, suggesting a directional influence of the brainstem on cortical delta. Such a possibility aligns with the broader literature on the potential role of the brainstem in QS regulation (Anaclet and Fuller, 2017).

Does respiration modulate delta?

Beginning at birth in rats, respiration is strongly modulated during sleep such that it is regular during QS and irregular during AS (Saini and Pagliardini, 2017). Thus, respiratory regularity is already a characteristic feature of QS when delta emerges at P12. If respiration entrains delta (Tort et al., 2018; Karalis and Sirota, 2022), then respiratory regularity may be a necessary condition for its expression. Furthermore, regular respiration may support the long-range synchronization of neural oscillations (Tort et al., 2018), especially low-frequency oscillations like delta. However, even if respiration entrains delta, the reverse may also be true: Indeed, it is likely most accurate to consider respiration and delta as coupled oscillators that bidirectionally influence each other across time and behavioral states (Braendholt et al., 2023).

Although respiratory and delta frequencies in P12 rats exhibit similar peak values of ~2 Hz (Ahmad et al., 2024), only the respiratory rate varies widely across species. Specifically, whereas respiratory frequency scales with body mass and metabolic rate (Buzsaki et al., 2013; Fahlman et al., 2025), delta frequency is highly conserved across species, occupying a narrow frequency band despite order-of-magnitude differences in body size. Thus, respiration is more likely to modulate delta than drive its rhythmicity.

A surprising finding of this study is the coupling of respiratory amplitude with delta power in response to sleep deprivation and hypercapnia. We selected hypercapnia as a second perturbation because it is an effective way to perturb the respiratory system (Almanza-Hurtado et al., 2022). In adult humans and rats, hypercapnia typically increases respiratory frequency and amplitude (Saetta and Mortola, 1985; Wickstrom et al., 2002; Molkov et al., 2014; Driver et al., 2016; Leirao et al., 2018). At P12, whereas hypercapnia produced marked increases in respiratory frequency across behavioral states, respiratory amplitude did not increase during wakefulness or AS and actually decreased during QS. Developmental differences in respiratory control during hypercapnia may explain these findings (Stunden et al., 2001; Putnam et al., 2005; Holley et al., 2012). Regardless, the observation that hypercapnia selectively reduced both respiratory amplitude and delta power during QS suggests a functional coupling between respiratory and delta-generating networks.

Our findings might suggest directional effects of respiratory amplitude on delta power. However, a potential confound is that hypercapnia also induces cerebrovascular dilation, which may alter neural activity independent of respiration (Hosford et al., 2022). Accordingly, we cannot discern at this time the causal pathway by which hypercapnia exerts its influence on delta.

That hypercapnia induces state-dependent changes in respiratory amplitude and state-independent changes in respiratory frequency may reflect the separate regulatory control of these two dimensions of the respiratory system (Del Negro et al., 2018; Krohn et al., 2023). Conditions of high sleep pressure or acute hypercapnia may therefore differentially engage these systems during early development. Given that mild hypercapnia (2% CO_2) consolidates QS in adult rats (Fraigne et al., 2008), future studies should assess how varying concentrations of inspired CO_2 differentially affect sleep and delta across development.

Together, these findings identify respiratory amplitude as a state-dependent physiological signal that is both homeostatically regulated and mechanistically coupled to delta power, revealing a previously unrecognized link between respiratory and sleep-homeostatic processes early in development.

How is delta orchestrated across the rostrocaudal axis?

Synchronization of spatially distant PZ and cortical delta necessitates common inputs. Two possible sources of delta driving inputs—one located rostrally and one caudally—may provide such coordination.

At the rostral end, the claustrum has emerged as a potential organizer of cortical delta (Smith et al., 2020). Across species—including rodents (Narikiyo et al., 2020) and humans (Lamsam et al., 2024)—the claustrum is implicated in the synchronization of cortical delta. Its extensive reciprocal inhibitory cortical projections make it well suited for this role (Jackson et al., 2020; Smith et al., 2020). An important unanswered question is whether the claustrum also coordinates delta activity beyond the cortex, including in structures like PZ.

At the caudal end, respiratory motor and sensory pathways provide a second possible source of coordination (Kubin et al., 2006; Zoccal et al., 2014; Krohn et al., 2023). There is evidence

that respiratory frequency entrains adult brain rhythms, including cortical delta (Ito et al., 2014; Biskamp et al., 2017; Tort et al., 2018). Such entrainment may occur indirectly via olfactory pathways or directly via brainstem respiratory signals (Karalis and Sirota, 2022). We showed previously that sectioning the olfactory nerve at P12 does not disrupt cortical delta (Ahmad et al., 2024), thus supporting bottom–up respiratory modulation (Karalis and Sirota, 2022). In addition to a possible influence from PZ, such bottom–up effects could arise from the ventral respiratory group, including the preBötzinger complex, which has numerous ascending projections (Yackle et al., 2017; Yang and Feldman, 2018). The nucleus of the solitary tract is another candidate structure as it receives respiratory input from the vagus nerve (Kubin et al., 2006; Holt, 2022) and the preBötzinger complex (Yang and Feldman, 2018) and has long been suspected to play a role in cortical EEG synchronization (Laguzzi et al., 1984; Anaclet and Fuller, 2017).

That cortical delta consistently lagged PZ delta provides some insight into their mutual influence. However, this finding cannot be taken as evidence of PZ delta driving cortical delta because there may be a third region driving both at different lags (Adhikari et al., 2010). Given the short lags and the lack of evidence of direct anatomical connectivity between the two structures (Su et al., 2018), it is possible that top–down and bottom–up influences jointly synchronize PZ and cortical delta. Such bidirectional coordination could provide stability and flexibility, allowing distributed delta networks to remain synchronized while responding dynamically to physiological and homeostatic demands.

Limitations

A limitation of the present study is its focus on a single developmental time point. Although P12 is developmentally significant, older ages should be studied to determine whether the phenomena reported here persist. A second limitation is that our assessment of PZ–cortical interactions was limited to LFP analyses because the perturbations used here—sleep deprivation and hypercapnia—introduced pronounced movement-related artifacts that prevented reliable tracking of single units across recording periods. A third limitation is that although our sleep-deprivation protocol was not intended to manipulate respiration, repeated arousing stimuli may themselves have altered breathing. Finally, stress could be a potential concern in studies involving sleep deprivation and hypercapnia; however, this concern is mitigated by the fact that rats between P4 and P14 exhibit minimal adrenocortical response to stressors (Walker et al., 1986; Dent et al., 2007).

Conclusions and future directions

By showing that two distinct experimental perturbations were unable to dissociate the expression of PZ and cortical delta, the present findings reinforce the notion that cortical delta is coupled with its brainstem counterpart. Furthermore, evoked parallel changes in respiration and delta power adds a new dimension to the notion that breathing and delta are intimately connected.

More broadly, this study provides a foundation for understanding how sleep, respiration, brain rhythms, and long-range functional connectivity are integrated early in development. By introducing hypercapnia as a tool for manipulating respiratory–delta coupling, we provide a new approach for probing brainstem–forebrain interactions during sleep. Future work should leverage these approaches to identify the circuits and mechanisms that synchronize distributed delta-generating regions and to determine how interactions between neural and physiological systems shape the developmental emergence of coherent brain states.

References

Abbey H, Howard E (1973) Statistical procedure in developmental studies on species with multiple offspring. Dev Psychobiol 6:329–335.

Abu-Shaweesh JM, Dreshaj IA, Thomas AJ, Haxhiu MA, Strohl KP, Martin RJ (1999) Changes in respiratory timing induced by hypercapnia in maturing rats. J Appl Physiol 87:484–490.

Adhikari A, Sigurdsson T, Topiwala MA, Gordon JA (2010) Cross-correlation of instantaneous amplitudes of field potential oscillations: a straightforward method to estimate the directionality and lag between brain areas. J Neurosci Methods 191:191–200.

Ahmad M, Kim J, Dwyer B, Sokoloff G, Blumberg MS (2024) Coincident development and synchronization of sleep-dependent delta in the cortex and medulla. Curr Biol 34:2570–2579.e5.

Allada R, Cirelli C, Sehgal A (2017) Molecular mechanisms of sleep homeostasis in flies and mammals. Cold Spring Harb Perspect Biol 9:a027730.

Almanza-Hurtado A, Polanco Guerra C, Martinez-Avila MC, Borre-Naranjo D, Rodriguez-Yanez T, Duenas-Castell C (2022) Hypercapnia from physiology to practice. Int J Clin Pract 2022:2635616.

Anaclet C, Lin JS, Vetrivelan R, Krenzer M, Vong L, Fuller PM, Lu J (2012) Identification and characterization of a sleep-active cell group in the rostral medullary brainstem. J Neurosci 32:17970–17976.

Anaclet C, Ferrari L, Arrigoni E, Bass CE, Saper CB, Lu J, Fuller PM (2014) The GABAergic parafacial zone is a medullary slow wave sleep-promoting center. Nat Neurosci 17:1217–1224.

Anaclet C, Fuller PM (2017) Brainstem regulation of slow-wave-sleep. Curr Opin Neurobiol 44:139–143.

Biskamp J, Bartos M, Sauer JF (2017) Organization of prefrontal network activity by respiration-related oscillations. Sci Rep 7:45508.

Borbely AA, Achermann P (1999) Sleep homeostasis and models of sleep regulation. J Biol Rhythms 14:557–568.

Braendholt M, Kluger DS, Varga S, Heck DH, Gross J, Allen MG (2023) Breathing in waves: understanding respiratory-brain coupling as a gradient of predictive oscillations. Neurosci Biobehav Rev 152:105262.

Buzsaki G, Logothetis N, Singer W (2013) Scaling brain size, keeping timing: evolutionary preservation of brain rhythms. Neuron 80:751–764.

Buzsaki G, Draguhn A (2004) Neuronal oscillations in cortical networks. Science 304:1926–1929.

Buzsaki G, Voroslakos M (2023) Brain rhythms have come of age. Neuron 111:922–926.

Del Negro CA, Funk GD, Feldman JL (2018) Breathing matters. Nat Rev Neurosci 19:351–367.

Dent G, Choi DC, Herman JP, Levine S (2007) GABAergic circuits and the stress hyporesponsive period in the rat: ontogeny of glutamic acid decarboxylase (GAD) 67 mRNA expression in limbic-hypothalamic stress pathways. Brain Res 1138:1–9.

Dijk DJ (2009) Regulation and functional correlates of slow wave sleep. J Clin Sleep Med 5:S6–S15.

Dooley JC, Sokoloff G, Blumberg MS (2021) Movements during sleep reveal the developmental emergence of a cerebellar-dependent internal model in motor thalamus. Curr Biol 31:5501–5511.e5.

Driver ID, Whittaker JR, Bright MG, Muthukumaraswamy SD, Murphy K (2016) Arterial CO_2 fluctuations modulate neuronal rhythmicity: implications for MEG and fMRI studies of resting-state networks. J Neurosci 36:8541–8550.

Fahlman A, et al. (2025) Phylogenetic allometric scaling of near basal breathing frequency in terrestrial, semi-aquatic and aquatic mammals. Exp Physiol 110:1349–1357.

Fraigne JJ, Dunin-Barkowski WL, Orem JM (2008) Effect of hypercapnia on sleep and breathing in unanesthetized cats. Sleep 31:1025–1033.

Frank MG, Morrissette R, Heller HC (1998) Effects of sleep deprivation in neonatal rats. Am J Physiol 275:R148–R157.

Frank MG, Heller HC (1997) Development of REM and slow wave sleep in the rat. Am J Physiol 272:R1792–R1799.

Girardeau G, Lopes-Dos-Santos V (2021) Brain neural patterns and the memory function of sleep. Science 374:560–564.

Glanz RM, Dooley JC, Sokoloff G, Blumberg MS (2021) Sensory coding of limb kinematics in motor cortex across a key developmental transition. J Neurosci 41:6905–6918.

Gramsbergen A, Schwartze P, Prechtl HF (1970) The postnatal development of behavioral states in the rat. Dev Psychobiol 3:267–280.
Holley HS, Behan M, Wenninger JM (2012) Age and sex differences in the ventilatory response to hypoxia and hypercapnia in awake neonatal, prepubertal and young adult rats. Respir Physiol Neurobiol 180:79–87.
Holt MK (2022) The ins and outs of the caudal nucleus of the solitary tract: an overview of cellular populations and anatomical connections. J Neuroendocrinol 34:e13132.
Hosford PS, et al. (2022) CO_2 signaling mediates neurovascular coupling in the cerebral cortex. Nat Commun 13:2125.
Isler JR, Thai T, Myers MM, Fifer WP (2016) An automated method for coding sleep states in human infants based on respiratory rate variability. Dev Psychobiol 58:1108–1115.
Ito J, Roy S, Liu Y, Cao Y, Fletcher M, Lu L, Boughter JD, Grun S, Heck DH (2014) Whisker barrel cortex delta oscillations and gamma power in the awake mouse are linked to respiration. Nat Commun 5:3572.
Jackson J, Smith JB, Lee AK (2020) The anatomy and physiology of claustrum-cortex interactions. Annu Rev Neurosci 43:231–247.
Jasmeen KS, Pagliardini S (2017) Breathing during sleep in the postnatal period of rats: the contribution of active expiration. Sleep 40:12.
Jenni OG, Borbely AA, Achermann P (2004) Development of the nocturnal sleep electroencephalogram in human infants. Am J Physiol Regul Integr Comp Physiol 286:R528–R538.
Karalis N, Sirota A (2022) Breathing coordinates cortico-hippocampal dynamics in mice during offline states. Nat Commun 13:467.
Krohn F, Novello M, van der Giessen RS, De Zeeuw CI, Pel JJM, Bosman LWJ (2023) The integrated brain network that controls respiration. eLife 12: e83654.
Kubin L, Alheid GF, Zuperku EJ, McCrimmon DR (2006) Central pathways of pulmonary and lower airway vagal afferents. J Appl Physiol 101:618–627.
Laguzzi R, Reis DJ, Talman WT (1984) Modulation of cardiovascular and electrocortical activity through serotonergic mechanisms in the nucleus tractus solitarius of the rat. Brain Res 304:321–328.
Lamsam L, et al. (2024) The human claustrum tracks slow waves during sleep. Nat Commun 15:8964.
Lazic SE, Essioux L (2013) Improving basic and translational science by accounting for litter-to-litter variation in animal models. BMC Neurosci 14:37.
Leemburg S, Vyazovskiy VV, Olcese U, Bassetti CL, Tononi G, Cirelli C (2010) Sleep homeostasis in the rat is preserved during chronic sleep restriction. Proc Natl Acad Sci U S A 107:15939–15944.
Leirao IP, Silva CA, Gargaglioni LH, da Silva GSF (2018) Hypercapnia-induced active expiration increases in sleep and enhances ventilation in unanaesthetized rats. J Physiol 596:3271–3283.
Molkov YI, Shevtsova NA, Park C, Ben-Tal A, Smith JC, Rubin JE, Rybak IA (2014) A closed-loop model of the respiratory system: focus on hypercapnia and active expiration. PLoS One 9:e109894.
Molle M, Born J (2011) Slow oscillations orchestrating fast oscillations and memory consolidation. Prog Brain Res 193:93–110.
Mordkoff JT (2019) A simple method for removing bias from a popular measure of standardized effect size: adjusted partial eta squared. Adv Methods Pract Psychol Sci 2:228–232.
Narikiyo K, Mizuguchi R, Ajima A, Shiozaki M, Hamanaka H, Johansen JP, Mori K, Yoshihara Y (2020) The claustrum coordinates cortical slow-wave activity. Nat Neurosci 23:741.
Nir Y, Staba RJ, Andrillon T, Vyazovskiy VV, Cirelli C, Fried I, Tononi G (2011) Regional slow waves and spindles in human sleep. Neuron 70:153–169.
Peres FF (2025) Effect sizes for nonparametric tests. Biochem Med 36:5–16.
Puentes-Mestril C, Roach J, Niethard N, Zochowski M, Aton SJ (2019) How rhythms of the sleeping brain tune memory and synaptic plasticity. Sleep 42:zsz095.
Putnam RW, Conrad SC, Gdovin MJ, Erlichman JS, Leiter JC (2005) Neonatal maturation of the hypercapnic ventilatory response and central neural CO_2 chemosensitivity. Respir Physiol Neurobiol 149:165–179.
Saetta M, Mortola JP (1985) Breathing pattern and CO_2 response in newborn rats before and during anesthesia. J Appl Physiol 58:1988–1996.
Saini JK, Pagliardini S (2017) Breathing during sleep in the postnatal period of rats: the contribution of active expiration. Sleep 40:12.
Seelke AM, Blumberg MS (2008) The microstructure of active and quiet sleep as cortical delta activity emerges in infant rats. Sleep 31:691–699.
Smith JB, Lee AK, Jackson J (2020) The claustrum. Curr Biol 30:R1401–R1406.
Steggerda JA, Mayer CA, Martin RJ, Wilson CG (2010) Effect of intermittent hypercapnia on respiratory control in rat pups. Neonatology 97:117–123.
Stunden CE, Filosa JA, Garcia AJ, Dean JB, Putnam RW (2001) Development of in vivo ventilatory and single chemosensitive neuron responses to hypercapnia in rats. Respir Physiol 127:135–155.
Su YT, Gu MY, Chu X, Feng X, Yu YQ (2018) Whole-Brain mapping of direct inputs to and axonal projections from GABAergic neurons in the parafacial zone. Neurosci Bull 34:485–496.
Todd WD, Gibson JL, Shaw CS, Blumberg MS (2010) Brainstem and hypothalamic regulation of sleep pressure and rebound in newborn rats. Behav Neurosci 124:69–78.
Tononi G, Cirelli C (2006) Sleep function and synaptic homeostasis. Sleep Med Rev 10:49–62.
Tort ABL, Brankack J, Draguhn A (2018) Respiration-entrained brain rhythms are global but often overlooked. Trends Neurosci 41:186–197.
Vyazovskiy VV, Riedner BA, Cirelli C, Tononi G (2007) Sleep homeostasis and cortical synchronization: II. A local field potential study of sleep slow waves in the rat. Sleep 30:1631–1642.
Walker CD, Perrin M, Vale W, Rivier C (1986) Ontogeny of the stress response in the rat: role of the pituitary and the hypothalamus. Endocrinology 118:1445–1451.
Walker MP (2009) The role of slow wave sleep in memory processing. J Clin Sleep Med 5:S20–S26.
Wickstrom R, Hokfelt T, Lagercrantz H (2002) Development of CO_2-response in the early newborn period in rat. Respir Physiol Neurobiol 132:145–158.
Yackle K, Schwarz LA, Kam K, Sorokin JM, Huguenard JR, Feldman JL, Luo L, Krasnow MA (2017) Breathing control center neurons that promote arousal in mice. Science 355:1411–1415.
Yang CF, Feldman JL (2018) Efferent projections of excitatory and inhibitory preBotzinger complex neurons. J Comp Neurol 526:1389–1402.
Zoccal DB, Furuya WI, Bassi M, Colombari DS, Colombari E (2014) The nucleus of the solitary tract and the coordination of respiratory and sympathetic activities. Front Physiol 5:238.